Supplementary Information (SI) for Inorganic Chemistry Frontiers.
This journal is © the Partner Organisations 2024

Supporting Information

Chirality Driven Amplification of Sensitive Polarized Light Detection in Alternating Cations-Intercalated Perovskites

Hang Li,[a,b] Tingting Zhu,[a] Qianwen Guan, [a,b] Huang Ye, [a] Shihai You, [a] Chengshu Zhang, [a] Yifei Wang, [a] Peng Wang, [a] Chengmin Ji, [a] and Junhua Luo*[a,b,c]

[a] State Key Laboratory of Structure Chemistry, Fujian Institute of Research on the Structure of Matter, Chinese Academy of Sciences, Fuzhou, Fujian, 350002, P. R. China. Email: jhluo@fjirsm.ac.cn

[b] University of Chinese Academy of Sciences, Beijing, 100049, China.

[c] Key Laboratory of Fluorine and Silicon for Energy Materials and Chemistry of Ministry of Education, School of Chemistry and Chemical Engineering, Jiangxi Normal University, Nanchang, Jiangxi 330022, China.

Experimental Section

Materials: (R)-(+)-1-Phenylpropylamine reagent (98%, Aladdin), lead(II) acetate trihydrate $Pb(Ac)_2 \cdot 3H_2O$ (99.5%, Aladdin), Ethylamine (EA,70% in water), hydrobromic acid(HBr, 40%, AR). All chemicals used have no further purification.

Synthesis and crystal growth: Lead (II) acetate trihydrate (2.63 mmol,1 g) is added to 10ml of concentrated hydrobromic acid and heated to complete dissolution, followed by the addition of R-1-Phenylpropylamine (5.26 mmol,0.72 g) and Ethylamine (9.52 mmol,0.3 g) to heat the solution under a constant magnetic stirrer until it is colorless and clear. The crystals are obtained by transferring the heated solution to the oven and slowly reducing it to room temperature at rate of 1.5 K day^{-1}.

Single crystal structure determination and Powder X-ray diffraction: Single crystal X-ray diffraction (XRD) experiments were performed on a Bruker APEX-II diffractometer with Mo Kα radiation, operating at 50 kV and 40 mA. The structures were solved by direct method and refined by full-matrix least-squares on F^2 using the SHELX package. The structure-solving and refinement processes were conducted in the Olex2 software. Powder X-ray diffraction(PXRD) data was obtained by Rigaku Miniflex600 powder X-ray diffractometer with the 2θ range of 5°-50° at room temperature.

Characterization: The data of powder X-ray diffraction (PXRD) is captured by utilizing the Rigaku MiniFlex diffractometer in 2θ range of 5°–50° that using a step size of 0.02° at room temperature. Method of using the DFT method within the total energy code CASTEP calculates the bandgap and partial density of states (PDOS). In the generalized gradient approximation, Perdew-Burke-Ernzerh take account into the exchange and correlation effects. The method of using norm-conserving pseudopotential characterizes the core-electron interactions between the ionic cores and electrons. The high cut-off energy of 910 eV and the k-point sampling of the Brillouin zone of 4 × 2 × 2 were set for **1**. Using the PE Lambda 950 UV-Visible spectrophotometer measures the optical ultraviolet-visible absorption spectrum at room

temperature. Thermogravimetric analysis is performed using a Netzsch STA449C thermal analyzer between 298K and 1200K, at a heating rate of 15 K min^{-1}.

Fabrication and measurement of polarized photoelectric detector: The two sides of the single crystal plane are coated with symmetrical silver electrodes. Two probes are placed on the coated electrodes, which are measured at room temperature by using the Keithley 6517B source meter. The continuous-wave lasers (ITC4001) of 405 nm is used for illuminate device. Quarter-wave plate and half-wave plate respectively are achromatic zero-order wave-plate (CASTECH) and achromatic waveplate (THORLABS).

Figure

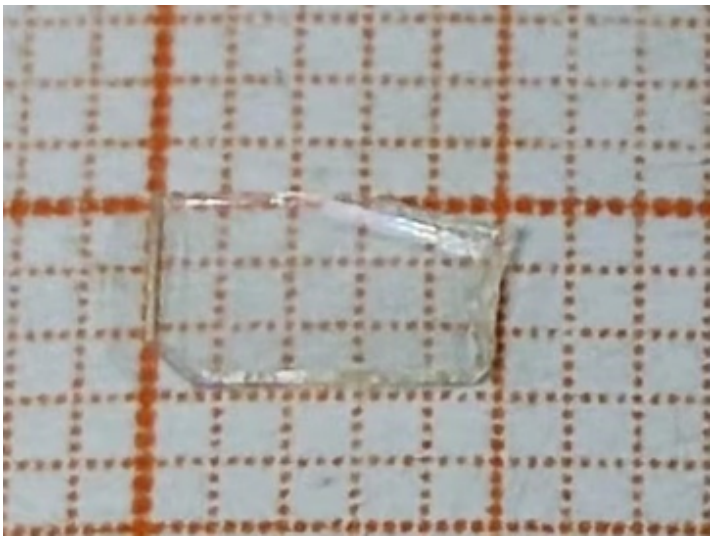

Figure S1 Crystal photo of **1**.

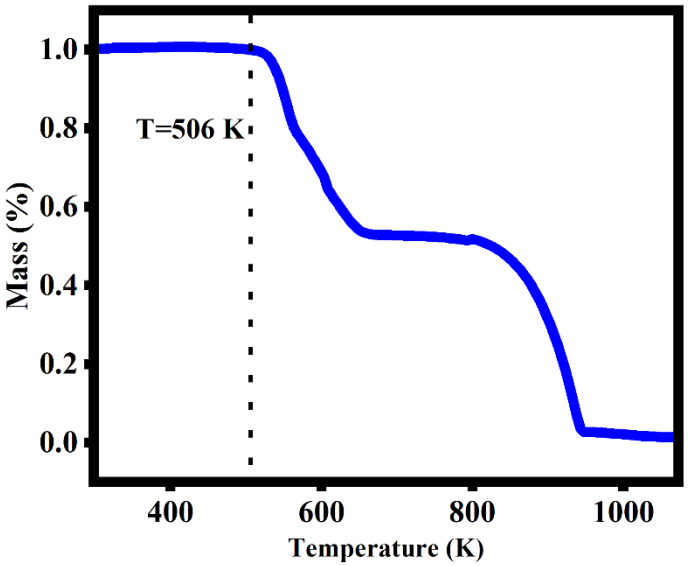

Figure S2. TG curve of **1** under nitrogen atmosphere.

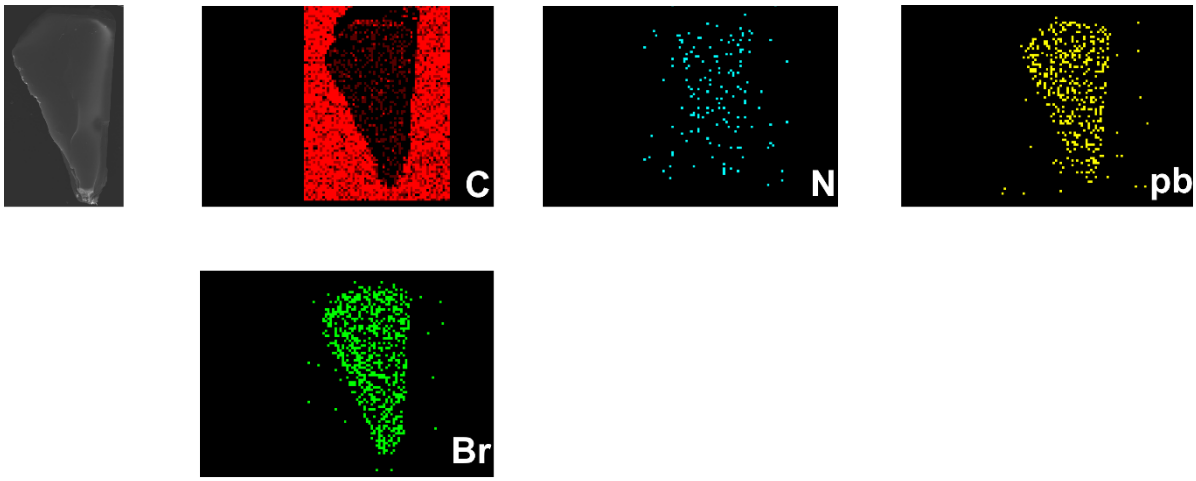

Figure S3. Energy-diffusive X-ray spectroscopy (EDS) mappings for Pb, Br, N, and C.

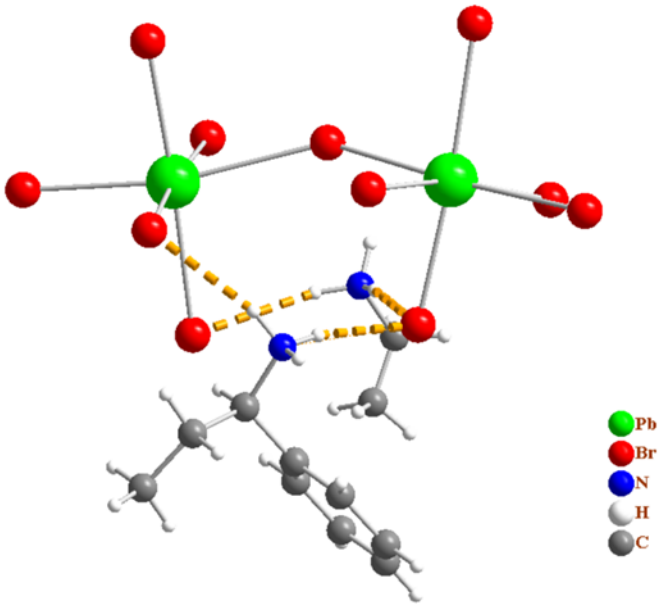

Figure S4. Schematic diagram of hydrogen bonding interactions between inorganic skeletons and organic cations.

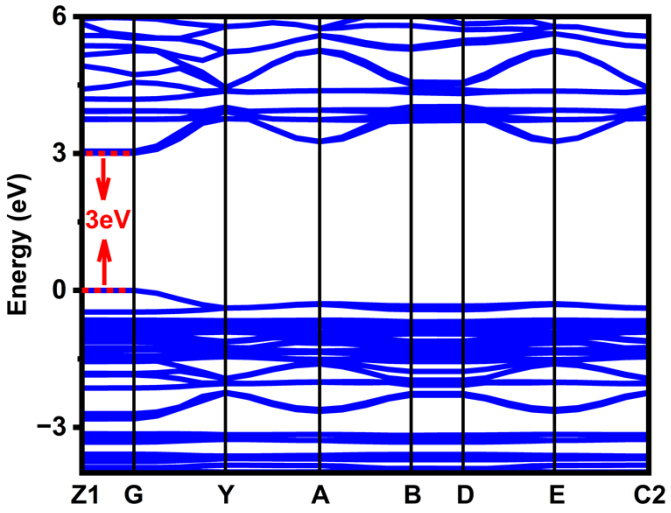

Figure S5. Calculated bandgap of **1**.

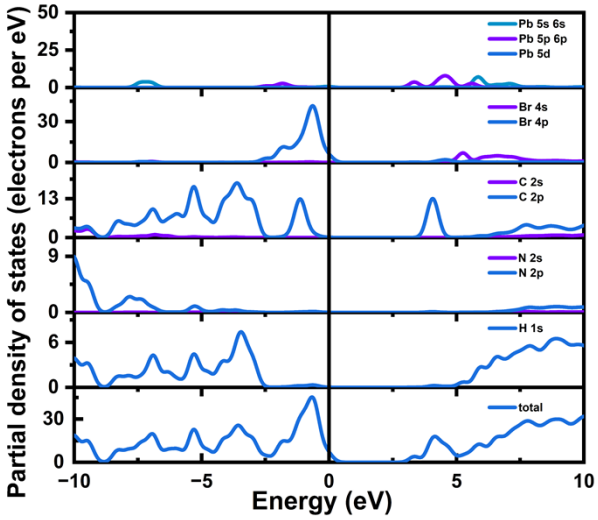

Figure S6. Partial density of states of **1** using the first-principles density functional theory.

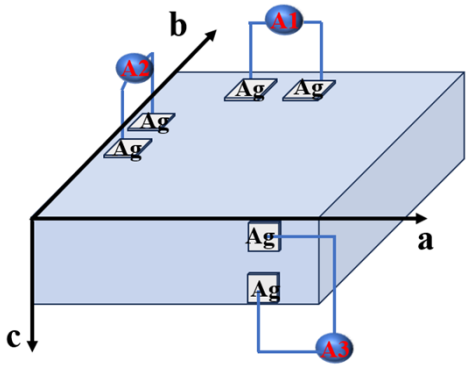

Figure S7. Conductivity measurement schematic diagram of **1**.

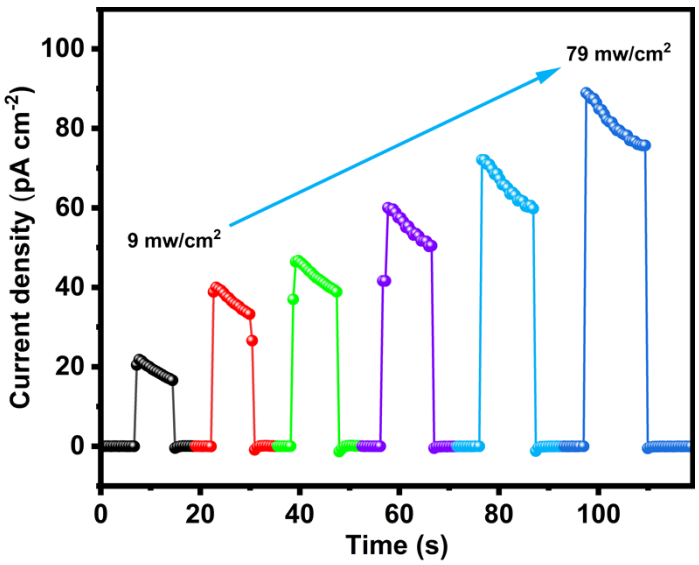

Figure S8. The current density of different power under 0 bias.

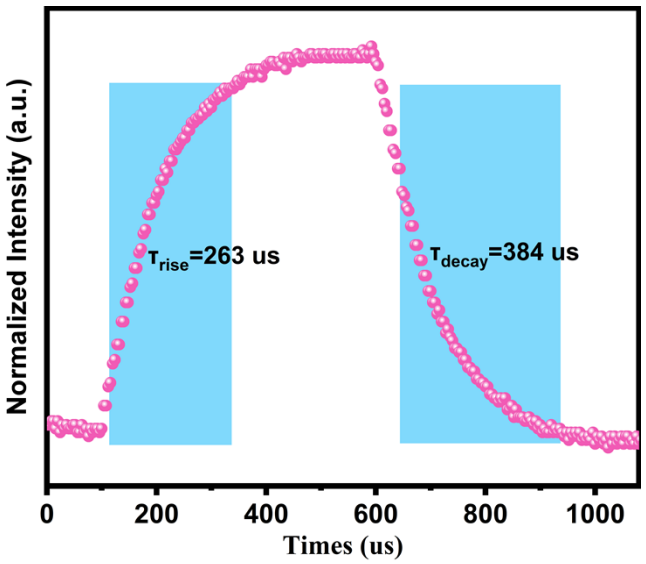

Figure S9. Rise and decay of photocurrent responses during on/off illumination switching.

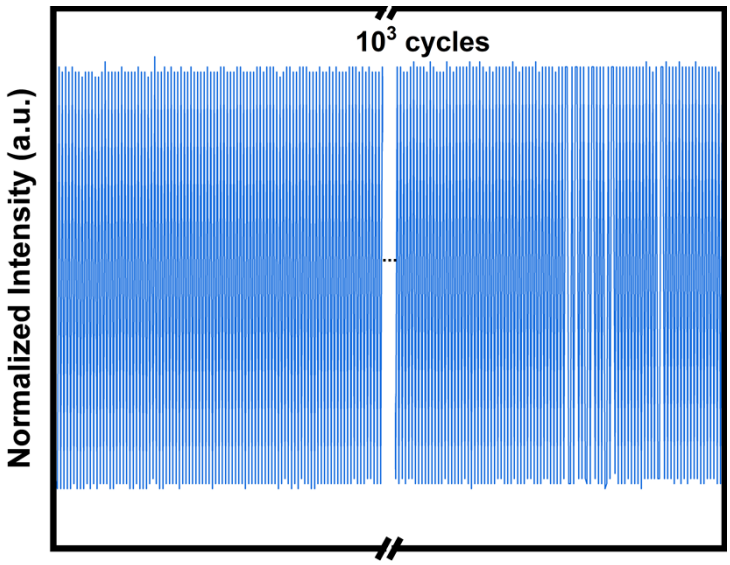

Figure S10. Repetitive switching cycles of time-dependent photoresponses of **1**.

Table S1. Polarization ratio of Some previously reported detectors with geometric anisotropy.

Device	BPVE	Polarization ratio	Ref
GeSe	-----	3.02	[1]
β-$GeSe_2$	-----	3.4	[2]
$GeAs_2$	-----	2	[3]
Black phosphorus	-----	0.59	[4]
o-SiP	-----	3.14	[5]
GeS_2	-----	2	[6]
$CH_3NH_3PbI_3$	-----	1.3	[7]
$CsPbI_3$	-----	2.6	[8]
CdSe	-----	0.75	[9]
$(BA)_2(GA)Pb_2I_7$ (BA = n-butylammonium, GA = guanidium).	-----	2.2	[10]
$(FPEA)PbI_4$ (FPEA = p-fluorophenethylammonium)	-----	2.1	[11]
$(TRA)_2CsPb_2Br_7$ (TRA = (carboxy)cyclohexylmethylammonium)	-----	2.1	[12]
$(CBA)_2CsPb_2Br_7$ (CBA = 4-chlorobenzyllamine)	0.2 V	2.7	[13]
$(BA)_2(FA)Pb_2I_7$ (BA = n-butylammonium, FA = formamidinium)	0.3 V	1.96	[14]
$(FPEA)_2(MA)Pb_2I_7$ (FPEA = 4-fluorophenethylammonium, MA = methylammonium)	0.4 V	3.15	[15]
$(i\text{-}BA)_2(MA)Pb_2I_7$ (i-BA = isobutylammonium, MA =	0.25 V	2.5	[16]

methylammonium)				
(R-PPA)(EA)$PbBr_4$ (R-PPA = phenylpropylamine, EA = ethylamine)	(R)-(+)-1-	0.07 V	3	This work

References

1 X. Wang, Y. Li, L. Huang, X.-W. Jiang, L. Jiang, H. Dong, Z. Wei, J. Li and W. Hu, Short-Wave Near-Infrared Linear Dichroism of Two-Dimensional Germanium Selenide., *J. Am. Chem. Soc.*, 2017, **139**, 14976–14982.

2 Y. Yang, S.-C. Liu, W. Yang, Z. Li, Y. Wang, X. Wang, S. Zhang, Y. Zhang, M. Long, G. Zhang, D.-J. Xue, J.-S. Hu and L.-J. Wan, Air-Stable In-Plane Anisotropic $GeSe_2$ for Highly Polarization-Sensitive Photodetection in Short Wave Region. *J. Am. Chem. Soc.*, 2018, **140**, 4150–4156.

3 L. Li, P. Gong, D. Sheng, S. Wang, W. Wang, X. Zhu, X. Shi, F. Wang, W. Han, S. Yang, K. Liu, H. Li and T. Zhai, Highly In-Plane Anisotropic 2D $GeAs_2$ for Polarization-Sensitive Photodetection. *Advanced Materials*, 2018, **30**, 1804541.

4 S. Zhao, J. Wu, K. Jin, H. Ding, T. Li, C. Wu, N. Pan and X. Wang, Highly Polarized and Fast Photoresponse of Black Phosphorus-InSe Vertical p–n Heterojunctions., *Adv Funct Materials*, 2018, **28**, 1802011.

5 X. Wang, Y. Cui, T. Li, M. Lei, J. Li and Z. Wei, Recent Advances in the Functional 2D Photonic and Optoelectronic Devices., *Advanced Optical Materials*, 2019, **7**, 1801274.

6 Y. Yang, S. Liu, X. Wang, Z. Li, Y. Zhang, G. Zhang, D. Xue and J. Hu, Polarization-Sensitive Ultraviolet Photodetection of Anisotropic 2D GeS_2., *Adv Funct Materials*, 2019, **29**, 1900411.

7 L. Gao, K. Zeng, J. Guo, C. Ge, J. Du, Y. Zhao, C. Chen, H. Deng, Y. He, H. Song, G. Niu and J. Tang, Passivated Single-Crystalline CH 3 NH 3 PbI 3 Nanowire Photodetector with High Detectivity and Polarization Sensitivity., *Nano Lett.*, 2016, **16**, 7446–7454.

8 Y. Zhou, J. Luo, Y. Zhao, C. Ge, C. Wang, L. Gao, C. Zhang, M. Hu, G. Niu and J. Tang, Flexible Linearly Polarized Photodetectors Based on All-Inorganic Perovskite CsPbI 3 Nanowires., *Advanced Optical Materials*, 2018, **6**, 1800679.

9 A. Singh, X. Li, V. Protasenko, G. Galantai, M. Kuno, H. (Grace) Xing and D. Jena, Polarization-Sensitive Nanowire Photodetectors Based on Solution-Synthesized CdSe Quantum-Wire Solids., *Nano Lett.*, 2007, **7**, 2999–3006.

10 L. Lu, Y. Ma, J. Wang, Y. Liu, S. Han, X. Liu, W. Guo, H. Xu, J. Luo and Z. Sun, Two-Dimensional Guanidine-Based Hybrid Perovskites with Strong Dichroism for Multiwavelength Polarization-Sensitive Detection., *Chemistry A European J*, 2021, **27**, 9267–9271.

11 M. Li, S. Han, B. Teng, Y. Li, Y. Liu, X. Liu, J. Luo, M. Hong and Z. Sun, Minute-Scale Rapid Crystallization of a Highly Dichroic 2D Hybrid Perovskite Crystal toward Efficient Polarization-Sensitive Photodetector., *Advanced Optical Materials*, 2020, **8**, 2000149.

12 Y. Liu, J. Wang, S. Han, X. Liu, M. Li, Z. Xu, W. Guo, M. Hong, J. Luo and Z. Sun, Multilayered 2D Cesium-Based Hybrid Perovskite with Strong Polarization Sensitivity: Dimensional Reduction of $CsPbBr_3$. *Chemistry A European J*, 2020, **26**, 3494–3498.

13 L. Wang, C. Wu, Z. Xu, H. Wu, X. Dong, T. Chen, J. Liang, S. Chen, J. Luo and L. Li, Realization of High-Performance Self-Powered Polarized Photodetection with Large Temperature Window in a 2D Polar Perovskite., *Small*, 2023, 2310166.

14 Z. Xu, X. Dong, L. Wang, H. Wu, Y. Liu, J. Luo, M. Hong and L. Li, Precisely Tailoring a $FAPbI_3$ -Derived Ferroelectric for Sensitive Self-Driven Broad-Spectrum Polarized Photodetection., *J. Am. Chem. Soc.*, 2023,

145, 1524–1529.

15 X. Hu, H. Xu, Y. Liu, L. Lu, W. Guo, S. Han, J. Luo and Z. Sun, Incorporating an Aromatic Cationic Spacer to Assemble 2D Polar Perovskite Crystals toward Self-Powered Detection of Quite Weak Polarized Light., *J. Phys. Chem. Lett.*, 2022, **13**, 6017–6023.

16 L. Lu, W. Weng, Y. Ma, Y. Liu, S. Han, X. Liu, H. Xu, W. Lin, Z. Sun and J. Luo, Anisotropy in a 2D Perovskite Ferroelectric Drives Self-Powered Polarization-Sensitive Photoresponse for Ultraviolet Solar-Blind Polarized-Light Detection., *Angew Chem Int Ed*., DOI:10.1002/anie.202205030.